Innate immune signaling in *Drosophila* shifts anabolic lipid metabolism from triglyceride storage to phospholipid synthesis in an ER stress dependent manner.

Brittany A. Martínez[1,2] and Michelle L. Bland[1,2]*

[1]Biomedical Sciences Graduate Program, and [2]Department of Pharmacology

University of Virginia, Charlottesville, VA 22908-0875

*Address correspondence to: Michelle L. Bland, mlb2eg@virginia.edu

ABSTRACT

During infection, cellular resources are allocated toward synthesis and secretion of effector proteins that neutralize and kill invading pathogens. In *Drosophila*, antimicrobial peptides (AMPs) are produced in the fat body, an organ that also serves as a major nutrient storage depot. Here we asked how the innate immune response activated by fat body Toll signaling alters lipid metabolism as a model for understanding how the cellular and energetic demands of the immune response are met. We find that genetic activation of fat body Toll signaling leads to a tissue-autonomous reduction in triglyceride storage that is paralleled by decreased transcript levels of *Lipin* and *midway*, enzymes that carry out the final steps of triglyceride synthesis. In contrast, Kennedy pathway enzymes that synthesize phospholipids and their products, phosphatidylcholine and phosphatidylethanolamine, are induced in fat bodies with active Toll signaling. Induction of these enzymes depends on the unfolded protein response mediator Xbp1, and examination of endoplasmic reticulum (ER) morphology by transmission electron microscopy revealed significantly expanded ER in fat body cells with active Toll signaling. Together these results indicate that Toll signaling induces a metabolic switch from triglyceride storage to phospholipid synthesis and ER expansion; this occurs in response to AMP production and may sustain AMP synthesis and secretion during infection. Better understanding of how this anabolic switch in lipid metabolism is induced, as well as the long-term consequences of reduced triglyceride storage at the expense of phospholipid synthesis, should yield insight into metabolic diseases that stem from chronic inflammation.

INTRODUCTION

The synthesis of antimicrobial peptides, acute phase proteins, and cytokines as well as cellular processes such as phagocytosis and immune cell proliferation lead to profound changes in host metabolism during the immune response. For example, mice injected with lipopolysaccharide (LPS) or infected with *Escherichia coli* exhibit trade-offs in core temperature and metabolism to drive disease tolerance (Ganeshan et al., 2019). At the level of individual immune cells, immune signaling shifts glucose metabolism from oxidative phosphorylation to aerobic glycolysis; this switch promotes immune effector functions (Chang et al., 2013; Gleeson et al., 2016; Krawczyk et al., 2010; Krejčová et al., 2019). Metabolic changes allow promote the secretory functions of immune cells. Upon simulation with LPS, mouse B cells differentiate into plasma cells that synthesize and secrete antibodies; this is accompanied by increased membrane phospholipid synthesis and the expansion of the endoplasmic reticulum (ER) (Fagone et al., 2007). Similarly, phosphatidylcholine synthesis in macrophages promotes cytokine secretion as well as survival of mice infected with *Streptococcus pneumoniae* (Tian et al., 2008).

The *Drosophila melanogaster* larval fat body is an excellent model to study interactions between immune signaling and metabolism. The larval fat body is a single cell-layer thick organ that coordinates both the synthesis of antimicrobial peptides via activation of the Toll and Imd signaling pathways as well as the storage of nutrients and growth of the animal via the activation of the insulin and mTOR signaling pathways (Arrese and Soulages, 2010; Buchon et al., 2014). In response to septic injury with Gram-positive bacteria or fungi, for example, activation of Toll receptors and the downstream NF-kB transcription factors dorsal and Dif in the fat body stimulate synthesis and secretion of micromolar quantities of antimicrobial peptides (AMPs)

(Buchon et al., 2014; Valanne et al., 2011). AMPs such as Drosomycin fight pathogens by inhibiting spore germination of filamentous fungi and by disrupting microbial membranes (Hanson et al., 2019). In the fed state, the insulin receptor activation in the fat body in response to *Drosophila* insulin-like peptides leads to activation of Akt and mTOR. These kinases stimulate protein synthesis, cell growth, and storage of dietary sugars as triglycerides and glycogen (Lehmann, 2018). The metabolic pathways that convert dietary nutrients to glycogen, fatty acids, triglycerides and phospholipids are highly conserved from flies to mammals. The integration of these innate immune and insulin signaling pathways in a single organ in the genetic model organism *Drosophila melanogaster* allows for identification of genetic pathways that mediate interactions between the immune system and metabolism.

Activation of innate immune signaling in the *Drosophila* fat body disrupts lipid metabolism. Infection of adult flies with the intracellular bacterial pathogen *Mycobacterium marinarum* leads to a progressive depletion of whole-animal triglyceride stores concomitant with lipid accumulation in phagocytes that harbor mycobacteria (Dionne et al., 2006; Péan et al., 2017). Similarly, infection of adult flies with the intracellular parasite *Tubulinosema ratisbonensis* leads to colonization of fat body cells and impairs triglyceride storage, directing host fatty acids to fuel parasite growth (Franchet et al., 2019). Lipid storage defects can be elicited by genetic activation of the Toll and Imd pathways, indicating that metabolic changes are dictated not only by pathogen interaction but also by signaling from the host immune system. Expression of a constitutively-active Toll receptor, $Toll^{10b}$, in larval fat body inhibits whole-animal growth, disrupts insulin signaling in fat body, and reduces triglyceride storage (DiAngelo et al., 2009; Roth et al., 2018; Suzawa et al., 2019). Similarly, activation of the Imd pathway in larval fat

body results in decreased triglyceride levels and impaired whole-animal growth (Davoodi et al., 2019).

The mechanism underlying altered lipid metabolism in response to infection and immune signaling and the consequences of such metabolic changes are unknown. To address this question, we activated Toll signaling in the larval fat body and assessed expression of enzymes that carry out de novo lipogenesis and triglyceride synthesis. We find that the decrease in triglycerides caused by chronic Toll signaling is mirrored by a selective decrease in expression of enzymes necessary to carry out *de novo* lipogenesis: the phosphatidic acid phosphatase Lipin and the diacylglycerol transferase homolog midway. Enzymes that carry out fatty acid synthesis are unchanged in response to Toll signaling, leading us to investigate other fates of fatty acids. We find an increase in phosphatidylethanolamine and phosphatidylcholine species and an increase in expression of enzymes in the Kennedy phospholipid synthesis pathway in fat bodies with active Toll signaling. The transcription factor X-box binding protein 1 (Xbp1) is required for induction of Kennedy pathway enzymes in fat bodies expressing constitutively-active $Toll^{10b}$, prompting us to examine the ER in fat bodies with active immune signaling. We find that the ER is expanded and dilated in fat body cells with active Toll signaling, suggesting that the secretory response elicited by the Toll pathway induces membrane phospholipid synthesis to drive ER secretory capacity.

RESULTS

Toll signaling in fat body acts in a tissue-autonomous manner to disrupt nutrient storage

The fat body stores the bulk of triglycerides in fruit fly larvae. Toll signaling in the larval fat body reduces whole-animal triglycerides, and we investigated whether this occurred in a fat body-specific manner. Activating Toll signaling in larval fat body decreased late third instar fat body triglyceride levels by 55%, but led to negligible changes in gut and carcass triglycerides compared with tissues from control larvae expressing GFP in fat body (Figure 1A). We also note, as expected, that the fat body stored 60-80 times more triglyceride than the gut and the carcass, which consists of cuticle, muscle, oenocytes, and attached tissues such as imaginal discs and trachea. We next asked whether the decrease in triglycerides in larvae expressing $Toll^{10b}$ in fat body was evident early in the third instar and whether it persisted in white prepupae, a well-defined developmental endpoint. Throughout the third instar larval stage, from 72 hours after egg lay to the formation of white prepupae, animals with active Toll signaling in the fat body consistently stored lower amounts of triglycerides compared with GFP controls. This held true whether triglyceride levels were normalized to whole-animal protein levels (Figure 1B) or body weight (Figure S1A). We find no significant decreases in whole-animal protein in larvae expressing $Toll^{10b}$ compared with controls over the same time course (Figure S1B). To understand whether the decrease in triglycerides elicited by innate immune signaling is a transcriptionally-regulated event, we manipulated the Nf-kB transcription factor Dif, which is activated by the Toll signaling pathway. Elevated expression of Dif in larval fat body phenocopied $Toll^{10b}$, leading to a decrease in whole-animal triglyceride levels (Figure 1C). However, loss of Dif in fat bodies with active Toll signaling rescued triglyceride storage (Figure 1D).

We investigated the underlying mechanism for reduced triglyceride storage in the immune-activated fat body beginning with examining levels of circulating glucose, the substrate for de novo fatty acid and triglyceride synthesis. Trehalose, a disaccharide composed of two glucose molecules, is the major circulating sugar in fruit flies. Hemolymph trehalose and glucose levels were equivalent in larvae expressing GFP or Toll^{10b} in fat body (Figure 2A), suggesting that altered substrate availability does not account for reduced triglyceride storage. Another fate of glucose is the branched polysaccharide glycogen. Surprisingly, whole-animal glycogen levels were increased in third instar larvae with active Toll signaling in fat body (Figure 2B). However, levels of glycogen were equivalent in white prepupae that expressed GFP or Toll^{10b} in fat body, and reduced from third instar levels, suggesting that some of the accumulated glycogen supports the final molt (Figure 2C). Both fat body and muscles in the body wall store glycogen. We observed a 3.7-fold increase in glycogen levels in fat body but no change in glycogen in the carcass, which contains the body wall musculature, of animals with active fat body Toll signaling (Figure 2D).

Toll signaling negatively regulates dedicated steps of triglyceride synthesis

De novo lipogenesis is controlled in part by transcriptional regulation of genes encoding lipogenic enzymes (Wang et al., 2015). Transcripts encoding *ATP citrate lyase* (*ATPCL*), *Acetyl-CoA carboxylase* (*ACC*) and *Fatty acid synthase 1* (*FASN1*), enzymes that synthesize fatty acids from dietary sugars, were expressed at equivalent levels in control and Toll^{10b}-expressing fat bodies (Figure 3A). In contrast, Toll signaling in fat body led to 40-45% reductions in transcripts encoding *Lipin*, a phosphatidic acid phosphatase that synthesizes diacylglycerol from

phosphatidic acid (Figure 3B), and *midway*, the *Drosophila* homolog of diacylglycerol acetyltransferase (DGAT), that carries out the final step in triglyceride synthesis (Figure 3C).

Knockdown of Lipin or midway in fat body or loss of midway in the whole animal decreased triglyceride storage (Figures S2A-S2C), consistent with previous findings (Beller et al., 2010; Grillet et al., 2016; Schmitt et al., 2015; Ugrankar et al., 2011). Elevated fat body expression of Lipin or midway was not sufficient to drive triglyceride accumulation in otherwise wild type larvae (Figures S2D-S2F). However, fat body-specific expression of a UAS-midway transgene restored triglycerides in flies heterozygous for the mdy^{QX25} null mutation (Figure S2G).

We asked whether triglyceride storage could be rescued by forcing expression of either Lipin or midway in animals with active Toll signaling in fat body. Elevated Lipin failed to rescue low triglyceride levels in larvae co-expressing $Toll^{10b}$ (Figure 3D). Similarly, co-expression of a wild type midway transgene with $Toll^{10b}$ did not rescue triglyceride storage (Figure 3E). The failure of Lipin or midway expression to rescue low triglycerides in larvae with active innate immune signaling is consistent with the possibility that fatty acids are being diverted to another purpose in cells with active Toll signaling and that elevated flux through this second pathway prevents triglyceride accumulation.

Innate immune signaling induces phospholipid synthesis

Given that *ATPCL*, *ACC* and *FASN1* are expressed at normal levels in fat bodies with active Toll signaling, we considered that fatty acids produced by the actions of these enzymes might be used for purposes other than triglyceride storage during the immune response. A major fate of fatty

acids in cells is phospholipid synthesis via the Kennedy pathway (Figure 4A). We assessed transcript levels of Kennedy pathway homologs in fat bodies expressing GFP or Toll^{10b} under control of r4-GAL4. We find elevated transcript levels of *easily shocked* (*eas*), an ethanolamine kinase homolog, and *CG7149*, a *CEPT1* homolog, in fat bodies with active Toll signaling compared with controls (Figure 4B). *Phosphocholine cytidylyltransferase 1* (*Pcyt1*), a homolog of human *PCYT1A*, was induced by Toll signaling, while the choline kinase homolog *CG2201* was inconsistently increased by fat body Toll pathway activation (Figures 4C and S3A). Other enzymes in the Kennedy pathway, such as *Pect* and *bbc* (Figures 4B,C) and *Pcyt2* and *CG33116* (Figure S3B) were not induced by Toll signaling. Protein levels of eas and Pcyt1 were highly induced in fat bodies with active Toll signaling (Figures 4D,E). To determine the functional consequences of increased *eas*, *CG7149, CG2201*, and *Pcyt1* expression in fat bodies with active Toll signaling, we used mass spectrometry to measure levels of the major phosphatidylethanolamine (PE) and phosphatidylcholine (PC) species in fat body (Carvalho et al., 2012; Guan et al., 2013; Palm et al., 2012). Consistent with increased expression of Kennedy pathway enzymes, levels of most major PE and PC species were increased 1.5- to 2-fold in Toll^{10b}-expressing fat bodies compared with controls (Figure 4F).

Transcriptional control of Kennedy pathway enzymes in cells with active Toll signaling

We next investigated the role of two transcription factors – Sterol regulatory element binding protein (SREBP) and X box binding protein-1 (Xbp1) – in the elevated expression of phospholipid synthesizing enzymes in fat bodies with active Toll signaling. In flies, as in mammals, the transcription factor SREBP is a key regulator of de novo lipogenesis (Horton et al., 2002). We find that fat bodies expressing Toll^{10b} exhibit elevated expression of SREBP

mRNA and protein (Figure S4A,B). However, fat body-specific knockdown of SREBP did not affect either basal or Toll signaling-induced expression of *eas*, *CG7149*, or *CG2201*. Basal expression of *Pcyt1* was reduced nearly three-fold by loss of SREBP. However, activation of Toll signaling led to 1.8-fold induction of *Pcyt1* in fat bodies regardless of SREBP levels (Figure S4C).

The unfolded protein response mediator X box binding protein-1 (Xbp1) regulates de novo lipogenesis of membrane phospholipids to permit ER expansion (Sriburi et al., 2004). Xbp1 is activated by Ire1-mediated splicing (Cox and Walter, 1996; Plongthongkum et al., 2007), and fat bodies with active Toll signaling exhibit elevated levels of spliced *Xbp1* compared with controls (Figure 5A and S4D). *Xbp1* null mutants die as second instar larvae (Ryoo et al., 2007), and chronic knockdown of *Xbp1* in larval fat body via r4-GAL4 strongly inhibits whole-animal growth (data not shown). However, acute induction of both $Toll^{10b}$ and $Xbp1^{RNAi}$ transgenes in fat body using TubGAL80ts to restrict r4-GAL4 expression in a temperature-dependent manner led to a near-complete loss of *Xbp1* transcripts. In addition, knocking down *Xbp1* blocked $Toll^{10b}$-dependent induction of *SREBP*, *eas* and *CG7149* (Figure 5A). Acute loss of *Xbp1* in fat body reduced basal levels of *Pcyt1* transcripts, as was the case with chronic loss of SREBP (refer back to Figure S4C). However, Toll signaling induced *Pcyt1* only 1.2-fold in fat bodies with acute loss of *Xbp1*. We did not observe induction of *CG2201* in this experiment, perhaps due to the acute nature of $Toll^{10b}$ expression (Figure 5A). Finally, acute loss of *Xbp1* blunted induction of the AMP *Drs* by Toll signaling; we did not observe changes in *Drs* when SREBP was manipulated (Figures 5A and S4D).

Toll signaling leads to ER expansion

The induction of Xbp1 splicing in fat bodies with active innate immune signaling suggested that the ER unfolded protein response might be induced in this situation. We therefore examined expression of canonical ER resident proteins that participate in the unfolded protein response and found significantly elevated expression of *binding immunoglobulin protein* (*BiP*), *protein disulfide isomerase* (*PDI*), and *ER degradation enhancer mannosidase alpha-like 1* (*Edem1*) in response to chronic Toll signaling (Figure 5B).

To examine whether ER morphology is altered by innate immune signaling, we used transmission electron microscopy to analyze fat bodies expressing GFP or Toll^{10b}. We observed dilated ER in fat body cells with active Toll signaling compared with controls (Figure 5C). To quantify this difference, we used stereological tools to compare organelles and features such as glycogen and cytosol between genotypes. This revealed a 40% increase in ER volume density with a simultaneous 40% decrease in organelle-free cytosol in response to Toll pathway activation. We find no significant difference in the volume density of lipid droplets, but we observe an increase in glycogen volume (Figure 5D).

AMP synthesis contributes to induction of Kennedy pathway enzymes

During the immune response to fungi or Gram-positive bacteria, the Toll signaling pathway drives synthesis and secretion of large quantities of AMPs. Individual AMPs have been measured at levels close to 100 μM in hemolymph, which represents secretion of millions of individual proteins (Fehlbaum et al., 1994). AMPs are secreted by fat body cells via the classical ER-Golgi-secretory vesicle pathway (Shandala et al., 2011). Acute activation of Toll signaling

leads to three-fold or greater induction of 17 of the 37 AMPs encoded in the *Drosophila* genome (Suzawa et al., 2019). We reasoned that ER expansion and phospholipid synthesis may serve the process of AMP production and secretion. To test this hypothesis, we asked whether induction of Kennedy pathway enzymes occurs downstream of AMP synthesis. The $Bom^{\Delta 55C}$ mutation deletes a cluster of ten highly-induced genes, the bomanins, that are critical for survival during infection (Clemmons et al., 2015), and the $Drs^{\Delta 7\text{-}17}$ mutation is a deletion of *Drs* (Kenmoku et al., 2017). Together, the genes encoded in the Bom^{55C} cluster and *Drs* account for 80% of the AMP transcripts that are induced by Toll signaling (Figure S5A). We drove $Toll^{10b}$ in fat bodies of flies with or without $Bom^{\Delta 55C}$ and $Drs^{\Delta 7\text{-}17}$ mutations and measured expression of *eas* and *Pcyt1*. The $Bom^{\Delta 55C}$ and $Drs^{\Delta 7\text{-}17}$ mutations, alone or in combination, led to the expected decreases in $Toll^{10b}$-induced expression of *BomS2* and *Drs* (Figures 6A,B). Unmanipulated AMPs such as *IM4* and *IM14* were still induced by $Toll^{10b}$ in $Bom^{\Delta 55C}$ and $Drs^{\Delta 7\text{-}17}$ single or double mutants (Figure S5B). In larval fat bodies expressing GFP, mutation of $Bom^{\Delta 55C}$ and $Drs^{\Delta 7\text{-}17}$ did not alter basal levels of *eas* or *Pcyt1*. However, $Bom^{\Delta 55C}; Drs^{\Delta 7\text{-}17}$ double homozygotes expressing $Toll^{10b}$ exhibited only a 1.6-fold induction of *eas* and a 1.3-fold induction of *Pcyt1*. In contrast, in larvae with a full complement of AMPs, Toll signaling elicited a 4.1-fold induction of *eas* and a 2.1-fold induction of *Pcyt1* (Figures 6C,D).

DISCUSSION

Here we show that chronic Toll pathway activity acts in a tissue-autonomous manner to impair triglyceride storage and increase phospholipid synthesis in the *Drosophila* larval fat body, an organ analogous to mammalian liver and adipose tissue. This decrease in triglycerides is not due to a decrease in availability of the substrate glucose; indeed, larvae with active Toll signaling exhibit a transient increase in fat body glycogen storage compared with controls. Transcript levels of *Lipin* and the DGAT homolog *midway*, enzymes that regulate the last steps of de novo lipogenesis, are selectively decreased in fat bodies expressing active Toll receptors, mirroring decreased triglyceride levels. Another fate of fatty acids is phospholipid synthesis, and fat bodies with active Toll signaling show tissue-autonomous increases in levels of major PE and PC species. Kennedy pathway enzymes that synthesize PE and PC are increased at the transcript and protein level in larvae with active Toll signaling in the fat body, mirroring increased phospholipid levels. This increase in phospholipid enzyme transcripts is dependent on the transcription factor Xbp1, an important regulator of ER biogenesis and the unfolded protein response. Morphological analysis of the ER shows expanded and dilated ER in fat bodies with active Toll signaling. During infection and in response to Toll signaling, the animal makes massive quantities of antimicrobial peptides to defend against pathogenic Gram-positive bacteria and fungi. AMPs are synthesized and secreted from the fat body during infection. We show that deletion of AMP genes blunts the Toll-dependent induction of key enzymes that synthesize phospholipids, suggesting that elevated synthesis of these secreted proteins, and possibly ER stress, contributes to induction of the Kennedy pathway. These data suggest that the animal must induce expression of enzymes that synthesize membrane phospholipids in order to sustain synthesis and secretion of AMPs at a high level within the secretory pathway.

Our results demonstrate a reciprocal relationship between triglyceride and phospholipid levels in the *Drosophila* larval fat body. Activating innate immune signaling in this organ leads to a decrease in triglyceride storage and increases in PE and PC species. Such a tradeoff between triglyceride storage and membrane phospholipid accumulation is observed in other contexts. In S2 cells, adult flies, and in *C. elegans*, loss of Kennedy pathway enzymes leads to elevated triglyceride levels (Guo et al., 2008; Lim et al., 2011; Walker et al., 2011). In contrast, manipulations that reduce lipin and DGAT activity directly or indirectly by disrupting Torsin function lead to elevated phospholipid levels and reduced triglyceride synthesis (Grillet et al., 2016; Yang et al., 2020). These studies and ours suggest that cells tightly regulate the balance between stored neutral lipids and membrane phospholipids.

Innate immune signaling in fat body shifts the balance between triglyceride accumulation and phospholipid synthesis, and our data suggest that this occurs at least in part by altering expression of key lipogenic enzymes. We find reduced *Lipin* and *midway* expression and elevated eas and Pcyt1 protein levels in fat bodies expressing constitutively-active Toll receptors. We were unable to rescue reduced triglyceride storage caused by Toll signaling by individually re-expressing Lipin or midway in fat body. A possible explanation for this result is that Lipin and midway must be expressed together to restore triglyceride synthesis in fat bodies expressing Toll^{10b}. It is also possible that Toll signaling disrupts subcellular localization of Lipin and/or midway such that transgenic expression of either or both enzymes would be insufficient to promote triglyceride accumulation. Flies with loss of the ER membrane protein Torsin exhibit an increase in nuclear Lipin and elevated triglyceride levels (Grillet et al., 2016), and in mammals,

insulin signaling promotes lipin activity by changing its subcellular distribution (Harris et al., 2007). Our previous work shows that Toll signaling in fat body inhibits insulin signaling, and that restoring insulin signaling rescues triglyceride storage (Roth et al., 2018). Therefore, Toll signaling might be expected to dominantly inhibit Lipin function by altering its subcellular distribution. Finally, the failure of forced Lipin or midway expression to restore triglyceride accumulation in fat bodies with active Toll signaling may be due to an increase in flux of fatty acids into the phospholipid synthesis pathway. Future work will be needed to distinguish among these possibilities.

Our results suggest that immune signaling leading to ER stress-induced synthesis of phospholipids and subsequent ER biogenesis that support the immune function is an ancient and conserved component of the immune response. The unfolded protein response is activated when high secretory demand leads to an abundance of misfolded proteins in the ER. In mice, ER stress induces splicing of Xbp1, and this response is required for immunoglobulin secretion in B cells (Kirk et al., 2010; Reimold et al., 2001). Membrane phospholipid synthesis underlies ER biogenesis during B cell differentiation (Fagone et al., 2007). Our data show that similar programs of Xbp1-dependent induction of phospholipid synthesis and ER expansion occur in response to Toll signaling in *Drosophila*. The signaling mechanisms linking Toll receptor activation with increased splicing of Xbp1 are unclear, but may depend on the increased synthesis of AMPs that would lead to ER stress. Indeed, we find that loss of AMP genes leads to a decrease in phospholipid synthesis enzymes, suggesting that a linear pathway exists between Toll, AMP synthesis, ER stress and Kennedy pathway enzyme induction.

The shift from nutrient storage to membrane phospholipid synthesis induced by Toll signaling likely has both immediate and long-term consequences for animal survival. The lipid metabolic switch accompanies ER expansion, and biogenesis of ER is predicted to sustain secretion of AMPs during infection. An increase in host PE and PC synthesis would lead to increased consumption of ethanolamine and choline. These molecules can be used as carbon and nitrogen sources for bacteria (Garsin, 2010; Romano et al., 2017), therefore increased host Kennedy pathway activity may lead to reduced growth for some species of bacteria. On the other hand, it is critical to tightly regulate ER function during infection because unrestrained Ire1 activity and Xbp1 splicing in *sigma-1 receptor* knockout mice leads to elevated proinflammatory cytokine production and increased rates of sepsis in response to LPS treatment (Rosen et al., 2019). A clear disadvantage of shifting fatty acids from nutrient storage to phospholipid synthesis in response to Toll signaling in flies is the large decrease in stored energy available for metamorphosis and early adult life. Animals with active Toll signaling enter the pupal stage with 50% of the amount of triglycerides that control animals store. Chronic activation of Toll signaling leads to a 80% decrease in adult viability, with most animals dying at the pharate adult stage (Roth et al., 2018). This decrease in viability is likely multifactorial, but impaired triglyceride levels likely lead to reduced metabolic energy to complete metamorphosis as well as a decrease in the pool of triglyceride that is needed to waterproof the adult cuticle (Storelli et al., 2019).

Together, our results show that Toll signaling leads to a profound change in lipid metabolism that supports immune function to fight infection but also hinders the ability of the animal to survive periods of reduced nutrient availability and high cellular demand for stored energy.

Future work defining how metabolic enzymes are regulated by innate immune signaling will further contribute to our understanding of metabolic diseases associated with inflammation and infection.

MATERIALS AND METHODS

Drosophila stocks and husbandry

Flies were raised on food containing 7.8% molasses, 2.4% yeast, 4.6% cornmeal, 0.3% propionic acid, and 0.1% methylparaben (Archon Scientific, Durham, NC). Except where noted, experiments were performed using mid- to late-third instar larvae (96-108 h after egg lay). The following stocks were obtained from the Bloomington *Drosophila* Stock Center (Bloomington, IN): UAS-RFP (#30556), UAS-GFP (2nd (#1521) and 3rd (#1522) chromosome insertions), UAS-Dif^{RNAi} (#30513), *mdy*^{QX25} (#5095), *mdy*^{EY07280} (#20167), UAS-midway^{RNAi} (#65963), UAS-Lipin^{RNAi} (#63614), UAS-Xbp1^{RNAi} (#36755), and r4-GAL4 (#33832). UAS-SREBP^{RNAi} (#37640) were obtained from the Vienna *Drosophila* Resource Center. Other flies used were: UAS-Toll^{10b} (Hu et al., 2004), UAS-Dif (Yagi and Ip, 2005), UAS-Lipin (Schmitt et al., 2015), *Bom*$^{\Delta 55C}$ (Clemmons et al., 2015), and *Drs*$^{\Delta 7\text{-}17}$ (Kenmoku et al., 2017).

Construction of UAS-HA.midway transgenic flies: The full-length *midway* cDNA was amplified by PCR from clone LD33582 (*Drosophila* Genomics Resource Center, Bloomington, IN) using gene-specific primers engineered to contain an amino-terminal HA tag (see Table 2). PCR products were cloned into pENTR (Invitrogen) and validated by sequencing. Gateway cloning (Invitrogen) was used to generate pUAST-HA.midway. This construct was injected into *Drosophila* embryos at Rainbow Transgenics (Camarillo, CA). Standard genetics was used to map and generate balanced transgenic lines.

Triglyceride and protein measurements: Whole larvae or dissected organs were flash frozen on dry ice. Samples were sonicated three times for 10 seconds each time in 140mM NaCl, 50mM

Tris-HCl, pH 7.4, 0.1% Triton X-100 with protease inhibitors (Roche). Following clearing by centrifugation at 4˚C, supernatants were transferred to new tubes. Triglyceride (Liquicolor Test, Stanbio) and protein (BCA assay, Pierce) were measured in each sample, and triglyceride levels were normalized to protein levels.

Hemolymph trehalose and glucose: Hemolymph was collected on ice from mid-third instar larvae (hemolymph from 8-10 larvae pooled per sample). Endogenous trehalase was destroyed by heating hemolymph diluted in PBS at 70˚C for 20 min. The sample was split in half, 1 mU trehalase (Sigma-Aldrich, T8778) was added to one tube, and both were incubated at 37˚C for 2h. Glucose was measured in both samples (GAGO20 kit, Sigma-Aldrich). Trehalose was calculated by subtracting glucose values in trehalase-free samples from glucose values in trehalase-treated samples, and then dividing by two as trehalose is a dimer of glucose. Trehalose and glucose values were normalized to hemolymph volume.

Glycogen and free glucose measurements: Whole larvae or dissected organs were flash frozen on dry ice. Samples were homogenized using a Kontes pestle in 0.1M NaOH. Following clearing by centrifugation at 4˚C, samples were incubated for 1h at 37˚C with 0.2M NaOAc, pH 4.8 with or without 5mg/mL amyloglucosidase (Sigma-Aldrich, A7420). Samples were then incubated for 10 min at room temperature with assay buffer including glucose oxidase (0.25 U/mL, Sigma-Aldrich, G7141) and horseradish peroxidase (0.17 U/mL, Sigma-Aldrich, P8250) and 20µM Amplex Red (Invitrogen, A36006). Fluorescence was measured (excitation/emission maxima = 535/587 nm) using an Infinite 200 PRO plate reader (Tecan). Glycogen was calculated as the amount of amyloglucosidase-hydrolyzed glucose, and free glucose is the amount of glucose

measured in the sample without hydrolysis via amyloglucosidase. Glycogen and free glucose levels were normalized first to glucose standards (Fisher CAS 50-99-7) and then to protein levels (BCA assay, Pierce).

Western blot analysis and antibodies: Fat bodies (n = 4-6 pooled/sample) were sonicated in lysis buffer (2% SDS, 60 mM Tris-HCl, pH 6.8) with phosphatase and protease inhibitors (Roche). Protein concentration was measured using a BCA assay (Pierce). Equal amounts of protein (10-40 µg/lane) were separated by SDS-PAGE, transferred to nitrocellulose, blocked in 3% milk in 1X TBS with 0.2% Tween 20 (TBS-T) and blotted overnight at 4˚C with primary antibodies diluted in 1% milk in TBS-T. Following multiple washes in TBS-T, secondary antibodies were incubated in 1% milk in TBS-T for 2h at room temperature, washed again, incubated with ECL (Pierce) and exposed to film. Antibodies used were: rabbit anti-human Histone H3, and rabbit anti-HA (4499 and 3724, Cell Signaling Technology); rabbit anti-*Drosophila* easily shocked (Pascual et al., 2005), guinea pig anti-*Drosophila* Pcyt1 (Grillet et al., 2016), mouse anti-human SREBP1 (SC-13551, Santa Cruz Biotechnology), rabbit anti-GFP (A11122, Inivtrogen), goat anti-rabbit HRP and goat anti-mouse HRP (111-035-003 and 115-035-003, Jackson ImmunoResearch), and goat anti-guinea pig HRP (6090-05, SouthernBiotech).

Quantitative RT-PCR: Total RNA was extracted from late third instar fat bodies (n = 4-6 pooled/sample) using a Direct-zol RNA MicroPrep kit (Zymo Research). DNAse-treated total RNA (1 µg) was used to generate cDNA using a High-Capacity cDNA Reverse Transcription kit (Thermo Fisher Scientific). Gene expression was measured using gene-specific primers. Quantitative PCR reactions were performed on 10-20 ng cDNA using SYBR Select Master Mix

(Thermo Fisher Scientific) with a Bio-Rad CFX Connect Real-Time PCR Detection System. Relative amounts of transcripts were calculated using the comparative Ct method with *Rp49* as a reference gene (Schmittgen and Livak, 2008). Table 1 lists gene-specific primer sequences.

Liquid chromatography and mass spectrometry: Larval fat bodies (n = 6 pooled/sample) were sonicated in ultrapure water and protein was measured (BCA assay, Pierce). Fat body lysates (normalized to 40 µg protein) underwent lipid extraction using a modified Bligh-Dyer method (chloroform: methanol: ultrapure water, ratio 2:2:1), adding 5µg 1,2-dinonadecanoyl-sn-glycero-3-phosphocholine (DNPC, Avanti Polar Lipids, 850320) to control for extraction efficiency. Organic extracts were dried and resuspended in chloroform: methanol (1:1) for quantification by liquid chromatography-coupled mass spectrometry. Lipids were separated on a EVO C18 column (Kinetex 5µm, 100 x 4.6 mm, Phenomenex), using a binary gradient consisting of Solvent A (69% methanol, 31% water with 10mM ammonium acetate) and Solvent B (50% methanol, 50% isopropanol with 10mM ammonium acetate) as the mobile phases. Phosphatidylcholine (PC) and phosphatidylethanolamine (PE) species identification and relative quantitation was achieved by liquid chromatography-linked electrospray ionization mass spectrometry on a 4000 Q Trap triple-quadrupole mass spectrometer (AB Sciex). Identification of phospholipids of interest, corresponding to PC and PE species with acyl chain lengths previously described to be abundant in larval fat body (Carvalho et al., 2012; Guan et al., 2013; Palm et al., 2012), was performed in positive ion mode via multiple reaction monitoring (Serbulea et al., 2018).

Electron Microscopy: Larval fat bodies were dissected and fixed initially in 2% glutaraldehyde, 2.5% formaldehyde, 0.1M Na cacodylate, pH 7.4 (30 min at room temperature followed by 1h on ice). They were then post-fixed in 1% OsO_4, 0.1M Na cacodylate, pH 7.4 (15 min on ice and 45 min at room temperature), washed three times for 5 min in 0.1M Na acetate, pH 6.0, and then stained in-block overnight at room temperature in 0.5% uranyl acetate in the same buffer. The samples were then dehydrated in acetone (70, 95, and 100%), exchanged from acetone into Epon resin, and embedded in fresh Epon. 70 nm sections from embedded fat bodies were mounted on copper grids, stained sequentially with uranyl acetate and lead citrate, and examined by transmission electron microscopy.

All images for stereology were taken in an unbiased manner at 6000X. Three different blocks of each genotype (r4>GFP or r4>$Toll^{10b}$) that each contained fat bodies from different animals were used for quantitative analysis, and each block was treated as a biological replicate. STEPanizer software (Java) was used for stereology analysis (Tschanz et al., 2011). In order to measure both volume density and surface area density, images were analyzed using nine-line tile pairs per image (Weibel et al., 1966). Point counts (volume density) and line intersections (surface area density) were made for organelles comprising the entire cytoplasmic landscape in each image. Batch mode was used to analyze images from each block for each genotype.

Quantitation and statistical analysis: Statistical parameters including exact sample sizes (with n referring to biological replicates), data plotted (typically mean ± SD), exact p values, and statistical tests used are reported in Figure Legends. Statistical analyses were performed using

Graphpad Prism 8. Data were analyzed by Student's t test or by one-way ANOVA with the Tukey-Kramer or Dunnett's multiple comparisons test.

ACKNOWLEDGEMENTS

We thank David Castle, Scott Yeudall, Norbert Letinger, Rosalie Hoyle and Young Jun Lee (all University of Virginia) for help with experiments. We thank Tony Ip (University of Massachusetts, Worcester), Michael Lehmann (University of Arkansas), Steven Wasserman (UCSD) and Takayuki Kuraishi (Kanazawa University, Japan) for flies, Thomas Preat (École des Neurosciences, Paris) for flies and the eas antibody, Rose Goodchild (KU Leuven, Belgium) for the Pcyt1 antibody. We thank Thurl Harris, Janet Cross (both University of Virginia) and members of the Bland lab for discussions. We thank the Bloomington *Drosophila* Stock Center and *Drosophila* Genomics Resource Center (both Bloomington, IN) and the Vienna *Drosophila* Resource Center (Vienna, Austria) for reagents. This work was supported by NIH Grant R01DK099601 to M.L.B. and Ruth L. Kirschstein NRSA Predoctoral Fellowship F31DK118879 to B.A.M.

REFERENCES

Arrese, E.L., Soulages, J.L., 2010. Insect Fat Body: Energy, Metabolism, and Regulation. Annu. Rev. Entomol. 55, 207–225. doi:10.1146/annurev-ento-112408-085356

Beller, M., Bulankina, A.V., Hsiao, H.-H., Urlaub, H., Jäckle, H., Kühnlein, R.P., 2010. PERILIPIN-Dependent Control of Lipid Droplet Structure and Fat Storage in Drosophila. Cell Metabolism 12, 521–532. doi:10.1016/j.cmet.2010.10.001

Buchon, N., Silverman, N., Cherry, S., 2014. Immunity in Drosophila melanogaster--from microbial recognition to whole-organism physiology. Nat. Rev. Immunol. 14, 796–810. doi:10.1038/nri3763

Carvalho, M., Sampaio, J.L., Palm, W., Brankatschk, M., Eaton, S., Shevchenko, A., 2012. Effects of diet and development on the Drosophila lipidome. Mol. Syst. Biol. 8. doi:10.1038/msb.2012.29

Chang, C.-H., Curtis, J.D., Maggi, L.B., Faubert, B., Villarino, A.V., O'Sullivan, D., Huang, S.C.-C., van der Windt, G.J.W., Blagih, J., Qiu, J., Weber, J.D., Pearce, E.J., Jones, R.G., Pearce, E.L., 2013. Posttranscriptional control of T cell effector function by aerobic glycolysis. Cell 153, 1239–1251. doi:10.1016/j.cell.2013.05.016

Clemmons, A.W., Lindsay, S.A., Wasserman, S.A., 2015. An effector Peptide family required for Drosophila toll-mediated immunity. PLoS Pathog. 11, e1004876. doi:10.1371/journal.ppat.1004876

Cox, J.S., Walter, P., 1996. A novel mechanism for regulating activity of a transcription factor that controls the unfolded protein response. Cell 87, 391–404.

DiAngelo, J.R., Bland, M.L., Bambina, S., Cherry, S., Birnbaum, M.J., 2009. The immune response attenuates growth and nutrient storage in Drosophila by reducing insulin signaling. Proc. Natl. Acad. Sci. U.S.A. 106, 20853–20858. doi:10.1073/pnas.0906749106

Dionne, M.S., Pham, L.N., Shirasu-Hiza, M., Schneider, D.S., 2006. Akt and FOXO dysregulation contribute to infection-induced wasting in Drosophila. Curr. Biol. 16, 1977–1985. doi:10.1016/j.cub.2006.08.052

Fagone, P., Sriburi, R., Ward-Chapman, C., Frank, M., Wang, J., Gunter, C., Brewer, J.W., Jackowski, S., 2007. Phospholipid biosynthesis program underlying membrane expansion during B-lymphocyte differentiation. J. Biol. Chem. 282, 7591–7605. doi:10.1074/jbc.M608175200

Fehlbaum, P., Bulet, P., Michaut, L., Lagueux, M., Broekaert, W.F., Hetru, C., Hoffmann, J.A., 1994. Insect immunity. Septic injury of Drosophila induces the synthesis of a potent antifungal peptide with sequence homology to plant antifungal peptides. J. Biol. Chem. 269, 33159–33163.

Franchet, A., Niehus, S., Caravello, G., Ferrandon, D., 2019. Phosphatidic acid as a limiting host metabolite for the proliferation of the microsporidium Tubulinosema ratisbonensis in Drosophila flies. Nat Microbiol 4, 645–655. doi:10.1038/s41564-018-0344-y

Ganeshan, K., Nikkanen, J., Man, K., Leong, Y.A., Sogawa, Y., Maschek, J.A., Van Ry, T., Chagwedera, D.N., Cox, J.E., Chawla, A., 2019. Energetic Trade-Offs and Hypometabolic States Promote Disease Tolerance. Cell 177, 399–413.e12. doi:10.1016/j.cell.2019.01.050

Garsin, D.A., 2010. Ethanolamine utilization in bacterial pathogens: roles and regulation. Nat. Rev. Microbiol. 8, 290–295. doi:10.1038/nrmicro2334

Gleeson, L.E., Sheedy, F.J., Palsson-McDermott, E.M., Triglia, D., O'Leary, S.M., O'Sullivan, M.P., O'Neill, L.A.J., Keane, J., 2016. Cutting Edge: Mycobacterium tuberculosis Induces

Aerobic Glycolysis in Human Alveolar Macrophages That Is Required for Control of Intracellular Bacillary Replication. J. Immunol. 196, 2444–2449. doi:10.4049/jimmunol.1501612

Grillet, M., Dominguez Gonzalez, B., Sicart, A., Pöttler, M., Cascalho, A., Billion, K., Hernandez Diaz, S., Swerts, J., Naismith, T.V., Gounko, N.V., Verstreken, P., Hanson, P.I., Goodchild, R.E., 2016. Torsins Are Essential Regulators of Cellular Lipid Metabolism. Dev. Cell 38, 235–247. doi:10.1016/j.devcel.2016.06.017

Guan, X.L., Cestra, G., Shui, G., Kuhrs, A., Schittenhelm, R.B., Hafen, E., van der Goot, F.G., Robinett, C.C., Gatti, M., González-Gaitán, M., Wenk, M.R., 2013. Biochemical Membrane Lipidomics during Drosophila Development. Dev. Cell 24, 98–111. doi:10.1016/j.devcel.2012.11.012

Guo, Y., Walther, T.C., Rao, M., Stuurman, N., Goshima, G., Terayama, K., Wong, J.S., Vale, R.D., Walter, P., Farese, R.V., 2008. Functional genomic screen reveals genes involved in lipid-droplet formation and utilization. Nature 453, 657–661. doi:10.1038/nature06928

Hanson, M.A., Dostálová, A., Ceroni, C., Poidevin, M., Kondo, S., Lemaitre, B., 2019. Synergy and remarkable specificity of antimicrobial peptides in vivo using a systematic knockout approach. Elife 8, 511. doi:10.7554/eLife.44341

Harris, T.E., Huffman, T.A., Chi, A., Shabanowitz, J., Hunt, D.F., Kumar, A., Lawrence, J.C., 2007. Insulin controls subcellular localization and multisite phosphorylation of the phosphatidic acid phosphatase, lipin 1. J. Biol. Chem. 282, 277–286. doi:10.1074/jbc.M609537200

Horton, J.D., Goldstein, J.L., Brown, M.S., 2002. SREBPs: activators of the complete program of cholesterol and fatty acid synthesis in the liver. J. Clin. Invest. 109, 1125–1131. doi:10.1172/JCI15593

Hu, X., Yagi, Y., Tanji, T., Zhou, S., Ip, Y.T., 2004. Multimerization and interaction of Toll and Spätzle in Drosophila. Proc. Natl. Acad. Sci. U.S.A. 101, 9369–9374. doi:10.1073/pnas.0307062101

Kenmoku, H., Hori, A., Kuraishi, T., Kurata, S., 2017. A novel mode of induction of the humoral innate immune response in Drosophila larvae. Dis Model Mech 10, 271–281. doi:10.1242/dmm.027102

Kirk, S.J., Cliff, J.M., Thomas, J.A., Ward, T.H., 2010. Biogenesis of secretory organelles during B cell differentiation. J. Leukoc. Biol. 87, 245–255. doi:10.1189/jlb.1208774

Krawczyk, C.M., Holowka, T., Sun, J., Blagih, J., Amiel, E., DeBerardinis, R.J., Cross, J.R., Jung, E., Thompson, C.B., Jones, R.G., Pearce, E.J., 2010. Toll-like receptor-induced changes in glycolytic metabolism regulate dendritic cell activation. Blood 115, 4742–4749. doi:10.1182/blood-2009-10-249540

Krejčová, G., Danielová, A., Nedbalová, P., Kazek, M., Strych, L., Chawla, G., Tennessen, J.M., Lieskovska, J., Jindra, M., Dolezal, T., Bajgar, A., 2019. Drosophila macrophages switch to aerobic glycolysis to mount effective antibacterial defense. Elife 8, 102. doi:10.7554/eLife.50414

Lehmann, M., 2018. Endocrine and physiological regulation of neutral fat storage in Drosophila. Mol. Cell. Endocrinol. 461, 165–177. doi:10.1016/j.mce.2017.09.008

Lim, H.Y., Wang, W., Wessells, R.J., Ocorr, K., Bodmer, R., 2011. Phospholipid homeostasis regulates lipid metabolism and cardiac function through SREBP signaling in Drosophila. Genes Dev. 25, 189–200. doi:10.1101/gad.1992411

Palm, W., Sampaio, J.L., Brankatschk, M., Carvalho, M., Mahmoud, A., Shevchenko, A., Eaton, S., 2012. Lipoproteins in Drosophila melanogaster—Assembly, Function, and Influence on Tissue Lipid Composition. PLoS Genet. 8, e1002828. doi:10.1371/journal.pgen.1002828.g008

Pascual, A., Chaminade, M., Preat, T., 2005. Ethanolamine kinase controls neuroblast divisions in Drosophila mushroom bodies. Dev. Biol. 280, 177–186. doi:10.1016/j.ydbio.2005.01.017

Péan, C.B., Schiebler, M., Tan, S.W.S., Sharrock, J.A., Kierdorf, K., Brown, K.P., Maserumule, M.C., Menezes, S., Pilátová, M., Bronda, K., Guermonprez, P., Stramer, B.M., Andres Floto, R., Dionne, M.S., 2017. Regulation of phagocyte triglyceride by a STAT-ATG2 pathway controls mycobacterial infection. Nat Commun 8, 14642. doi:10.1038/ncomms14642

Plongthongkum, N., Kullawong, N., Panyim, S., Tirasophon, W., 2007. Ire1 regulated XBP1 mRNA splicing is essential for the unfolded protein response (UPR) in Drosophila melanogaster. Biochem. Biophys. Res. Commun. 354, 789–794. doi:10.1016/j.bbrc.2007.01.056

Reimold, A.M., Iwakoshi, N.N., Manis, J., Vallabhajosyula, P., Szomolanyi-Tsuda, E., Gravallese, E.M., Friend, D., Grusby, M.J., Alt, F., Glimcher, L.H., 2001. Plasma cell differentiation requires the transcription factor XBP-1. Nature 412, 300–307. doi:10.1038/35085509

Romano, K.A., Martinez-Del Campo, A., Kasahara, K., Chittim, C.L., Vivas, E.I., Amador-Noguez, D., Balskus, E.P., Rey, F.E., 2017. Metabolic, Epigenetic, and Transgenerational Effects of Gut Bacterial Choline Consumption. Cell Host and Microbe 22, 279–290.e7. doi:10.1016/j.chom.2017.07.021

Rosen, D.A., Seki, S.M., Fernández-Castañeda, A., Beiter, R.M., Eccles, J.D., Woodfolk, J.A., Gaultier, A., 2019. Modulation of the sigma-1 receptor-IRE1 pathway is beneficial in preclinical models of inflammation and sepsis. Sci Transl Med 11, eaau5266. doi:10.1126/scitranslmed.aau5266

Roth, S.W., Bitterman, M.D., Birnbaum, M.J., Bland, M.L., 2018. Innate Immune Signaling in Drosophila Blocks Insulin Signaling by Uncoupling PI(3,4,5)P3 Production and Akt Activation. CellReports 22, 2550–2556. doi:10.1016/j.celrep.2018.02.033

Ryoo, H.D., Domingos, P.M., Kang, M.-J., Steller, H., 2007. Unfolded protein response in a Drosophila model for retinal degeneration. EMBO J. 26, 242–252. doi:10.1038/sj.emboj.7601477

Schmitt, S., Ugrankar, R., Greene, S.E., Prajapati, M., Lehmann, M., 2015. Drosophila Lipin interacts with insulin and TOR signaling pathways in the control of growth and lipid metabolism. J. Cell. Sci. 128, 4395–4406. doi:10.1242/jcs.173740

Schmittgen, T.D., Livak, K.J., 2008. Analyzing real-time PCR data by the comparative C(T) method. Nat Protoc 3, 1101–1108. doi:10.1038/nprot.2008.73

Serbulea, V., Upchurch, C.M., Schappe, M.S., Voigt, P., DeWeese, D.E., Desai, B.N., Meher, A.K., Leitinger, N., 2018. Macrophage phenotype and bioenergetics are controlled by oxidized phospholipids identified in lean and obese adipose tissue. Proc. Natl. Acad. Sci. U.S.A. 115, E6254–E6263. doi:10.1073/pnas.1800544115

Shandala, T., Woodcock, J.M., Ng, Y., Biggs, L., Skoulakis, E.M.C., Brooks, D.A., Lopez, A.F., 2011. Drosophila 14-3-3ε has a crucial role in anti-microbial peptide secretion and innate immunity. J. Cell. Sci. 124, 2165–2174. doi:10.1242/jcs.080598

Sriburi, R., Jackowski, S., Mori, K., Brewer, J.W., 2004. XBP1: A Link between the Unfolded Protein Response, Lipid Biosynthesis, and Biogenesis of the Endoplasmic Reticulum. J. Cell

Biol. 167, 35–41. doi:10.2307/1622293?refreqid=search-gateway:fc61de788ad47da65b3c86fd82749a3b

Storelli, G., Nam, H.-J., Simcox, J., Villanueva, C.J., Thummel, C.S., 2019. Drosophila HNF4 Directs a Switch in Lipid Metabolism that Supports the Transition to Adulthood. Dev. Cell 48, 200–214.e6. doi:10.1016/j.devcel.2018.11.030

Suzawa, M., Muhammad, N.M., Joseph, B.S., Bland, M.L., 2019. The Toll Signaling Pathway Targets the Insulin-like Peptide Dilp6 to Inhibit Growth in Drosophila. CellReports 28, 1439–1446.e5. doi:10.1016/j.celrep.2019.07.015

Tian, Y., Pate, C., Andreolotti, A., Wang, L., Tuomanen, E., Boyd, K., Claro, E., Jackowski, S., 2008. Cytokine secretion requires phosphatidylcholine synthesis. J. Cell Biol. 181, 945–957. doi:10.1083/jcb.200706152

Tschanz, S.A., Burri, P.H., Weibel, E.R., 2011. A simple tool for stereological assessment of digital images: the STEPanizer. J Microsc 243, 47–59. doi:10.1111/j.1365-2818.2010.03481.x

Ugrankar, R., Liu, Y., Provaznik, J., Schmitt, S., Lehmann, M., 2011. Lipin is a central regulator of adipose tissue development and function in Drosophila melanogaster. Mol. Cell. Biol. 31, 1646–1656. doi:10.1128/MCB.01335-10

Valanne, S., Wang, J.-H., Rämet, M., 2011. The Drosophila Toll signaling pathway. J. Immunol. 186, 649–656. doi:10.4049/jimmunol.1002302

Walker, A.K., Jacobs, R.L., Watts, J.L., Rottiers, V., Jiang, K., Finnegan, D.M., Shioda, T., Hansen, M., Yang, F., Niebergall, L.J., Vance, D.E., Tzoneva, M., Hart, A.C., Näär, A.M., 2011. A conserved SREBP-1/phosphatidylcholine feedback circuit regulates lipogenesis in metazoans. Cell 147, 840–852. doi:10.1016/j.cell.2011.09.045

Wang, Y., Viscarra, J., Kim, S.-J., Sul, H.S., 2015. Transcriptional regulation of hepatic lipogenesis. Nat. Rev. Mol. Cell Biol. 16, 678–689. doi:10.1038/nrm4074

Weibel, E.R., Kistler, G.S., Scherle, W.F., 1966. PRACTICAL STEREOLOGICAL METHODS FOR MORPHOMETRIC CYTOLOGY. J. Cell Biol. 30, 23–38. doi:10.1083/jcb.30.1.23

Yagi, Y., Ip, Y.T., 2005. Helicase89B is a Mot1p/BTAF1 homologue that mediates an antimicrobial response in Drosophila. EMBO Rep. 6, 1088–1094. doi:10.1038/sj.embor.7400542

Yang, C., Wang, X., Wang, J., Wang, X., Chen, W., Lu, N., Siniossoglou, S., Yao, Z., Liu, K., 2020. Rewiring Neuronal Glycerolipid Metabolism Determines the Extent of Axon Regeneration. Neuron 105, 276–292.e5. doi:10.1016/j.neuron.2019.10.009

FIGURE LEGENDS

Figure 1: Toll signaling in the third instar larval fat body reduces triglyceride storage in a tissue-autonomous manner.

r4-GAL4 was used to drive indicated transgenes in fat body, and triglyceride levels were measured in whole larvae or dissected organs and normalized to protein levels. (**A**) Triglyceride levels in fat body, gut, or carcass, n = 7-8/group. *p = 0.0118 and **p = 0.0047 versus GFP. (**B**) Whole-animal triglyceride levels throughout the third instar (72-120 hours after egg lay (h AEL)) and in white prepupae (WPP), n = 10-11/group. *p ≤ 0.0459 and **p ≤ 0.0019 versus GFP. (**C**) Whole-animal triglyceride levels in larvae expressing GFP or Dif in fat body, n = 7-8/group. *p = 0.0178 versus GFP. (D) Whole-animal triglyceride levels in larvae expressing GFP or $Toll^{10b}$+Dif^{RNAi} in fat body, n = 8/group. Data are presented as mean ± SD. p values were determined by Student's unpaired t test.

Figure 2. Toll signaling leads to increased fat body glycogen storage in the larval stage.

(**A**) Hemolymph glucose and trehalose levels in mid-third instar larvae expressing GFP or $Toll^{10b}$ in fat body under control of r4-GAL4, n = 4-5/group. (**B**) Late third instar whole-animal glycogen levels, normalized to protein, n = 12/group. ***p = 0.0002 versus GFP. (**C**) White prepupal whole-animal glycogen levels, normalized to protein, n = 14-17/group. (**D**) Glycogen levels in fat body and body wall, normalized to protein, from late third instar larvae expressing GFP or $Toll^{10b}$ in fat body, n = 11-13/group, ****p < 0.0001 versus GFP. Data are presented as means ± SD. p values were determined by Student's unpaired t test.

Figure 3. Reduced expression of *Lipin* and the DGAT homolog *midway* correlate with low triglyceride levels in larvae with active Toll signaling.

(**A-C**) Total RNA was extracted from late third instar larval fat bodies expressing GFP or Toll^{10b} under control of r4-GAL4. (**A**) *ATPCL*, *ACC*, and *FASN1* transcripts were measured by RT-qPCR and normalized to *Rp49*, n = 7/group. (**B**) *Lipin* mRNA levels in late third instar larval fat bodies expressing GFP or Toll^{10b}, n = 7/group. *p = 0.0259 versus GFP. (**C**) *mdy* mRNA levels in late-third instar larval fat bodies expressing GFP or Toll^{10b}, n = 7/group. **p = 0.0031 versus GFP. (**D**) Triglyceride levels in late third instar larvae expressing Toll^{10b} with or without a wild type Lipin transgene in fat body, n = 12/group. ****p < 0.0001 versus RFP+GFP. (**E**) Triglyceride levels in late third instar larvae expressing Toll^{10b} with or without a wild type mdy^{HA} transgene in fat body, n = 5-6/group. *p = 0.0156. Data are shown as mean ± SD. p values were determined by Student's t test (A-C) and one-way ANOVA with the Tukey-Kramer multiple comparisons test (D, E).

Figure 4. Toll signaling in fat body leads to a cascade of increased phospholipid synthesis enzymes and elevated membrane phospholipids.

(**A**) Schematic representation of phosphatidylethanolamine (PE) and phosphatidylcholine (PC) synthesis via the Kennedy pathway. (**B**) Late third instar fat body levels of *eas*, *Pect*, and *CG7149* transcripts, normalized to *Rp49*, n = 7/group. ***p ≤ 0.0002, ****p = 0.0001 versus GFP. (**C**) Late third instar fat body levels of *CG2201*, *Pcyt1*, and *bbc* transcripts, normalized to *Rp49*. n = 7/group. **p ≤ 0.0071 versus GFP. (**D, E**) Western blot analysis of eas (D) and Pcyt1 (E) protein levels in fat bodies expressing GFP or Toll^{10b} under control of r4-GAL4. Histone H3 levels are shown as loading controls. (**F**) Lipid extracts from late third instar larval fat bodies

expressing GFP or Toll^{10b} were used to quantify PE (left) and PC species (right), n = 6/group. *p < 0.05, **p < 0.01. Data are shown as mean ± SD. p values were determined by Student's unpaired t test.

Figure 5: Chronic fat body Toll signaling leads to expansion of the endoplasmic reticulum.

(**A**) Transcript levels of indicated genes were measured by RT-qPCR in late third instar larval fat bodies with GAL80ts-mediated induction of Toll^{10b} with or without Xbp1^{RNAi} for 24 hours at 30˚C, n = 6/group. *p < 0.05, **p < 0.01, ***p < 0.001, and ****p < 0.0001 versus fat bodies acutely expressing RFP+GFP. (**B**) Late third instar fat body levels of *BiP*, *PDI* and *Edem1* were measured by RT-qPCR and normalized to *Rp49*, n = 4-7/group, ***p = 0.001, ****p < 0.0001 versus GFP. (**C**) Electron micrographs of fat body cells expressing GFP (left) or Toll^{10b} (right) under control of r4-GAL4. ER, endoplasmic reticulum; LD, lipid droplet; g, glycogen; mt, mitochondria. Scale bar, 1 μm. (**D**) Stereological analysis of organelle- and feature-specific volume density. Data points represent the average of volume densities measured from 5-15 images from a single fat body, n = 4-5 fat bodies/group. *p = 0.0175, **p ≤ 0.0044 versus GFP. Data are presented as means ± SD. p values were determined by one-way ANOVA with Dunnett's multiple comparisons test (A) and Student's t test (B,D).

Figure 6. Induction of antimicrobial peptide synthesis contributes to regulation of eas and Pcyt1 by Toll signaling.

(**A,B**) Transcript levels of *Drs* (A) and *BomS2* (B), normalized to *Rp49*, in fat bodies of late third instar larvae expressing GFP (closed symbols) or Toll^{10b} (open symbols) under r4-GAL4 control. Animals were wild type, heterozygous, or homozygous for $Drs^{\Delta 7\text{-}17}$ and $Bom^{\Delta 55C}$ as indicated, n

= 5-8/group. *p = 0.0291, **p = 0.0015, ****p < 0.0001 versus GFP-expressing controls with the same $Drs^{\Delta 7\text{-}17}$ and $Bom^{\Delta 55C}$ genotypes. Note that GFP-expressing controls are heterozygous for $Drs^{\Delta 7\text{-}17}$ while Toll10b-expressing larvae are homozygous for $Drs^{\Delta 7\text{-}17}$. (**C, D**) Transcript levels of *eas* (**C**) and *Pcyt1* (**D**), normalized to *Rp49*, in fat bodies of late third instar larvae expressing GFP (closed symbols) or $Toll^{10b}$ (open symbols) under r4-GAL4 control. Animals were wild type, heterozygous, or homozygous for $Drs^{\Delta 7\text{-}17}$ and $Bom^{\Delta 55C}$ as indicated, n = 5-8/group (blue open and closed symbols) and n = 11-14/group for animals expressing GFP or $Toll^{10b}$ in fat body on a wild type background (black open and closed symbols). *p ≤ 0.0409, **p ≤ 0.032, ***p = 0.0009, ****p < 0.0001. Data are presented as means ± SD. p values were determined by Student's t test.

qRT-PCR primers, sequences listed 5' → 3'		
gene	**Forward primer**	**Reverse primer**
Rp49	CGCTTCAAGGGACAGTATCTG	AAACGCGGTTCTGCATGA
ATPCL	AAGGACATCCTGAACCGCCAT	GGCATTTCCGATCTTCTGGTC
ACC	CGCTATGGTTACCTGCCGTA	CGCTATGGTTACCTGCCGTA
FASN	GTGTTGGCCAACATTGACTAC	CTCAACAGTGTGTACTTCCAC
Lipin	GCGAGGTGATTGAGAAGAAG	AATGTTTGGGTCAGCTCGTG
midway	ACTGCTCTGCATTGGAGGTC	ATGTCCTTCGCCTTCGTTGT
eas	ACCAAACCCATGCCGATGAT	GGCGGCCGATAGGTAGAAAC
Pect	CAACGATGGAGGCAAATGGC	GGCATGTCCGAAGTGTACCA
CG7149	GAGGCTCATTTGAGGGGCTT	AGGGTGCATCACATAGACGC
CG2201	CACACAAACGTCAGCGATGC	ATTCGCAGAAGGACCTCACG
Pcyt1	TTACCTCAACGGCGTCAAGC	AAATTGTCGCAAAATCGGAGGC
bbc	GCGGTTCGGCAGAATTGATG	GACACTGGTGCCCTTGGTG
Pcyt2	AGCAATGGACAGAATGCCGA	GCAGGCTGGCAAATGCTAAAA
CG33116	ACGCAGGACCAGATCAATGG	CCAGCGCGGAAAGAACTTAAC
SREBP	CCTCTGCGATGAGTCGAGTG	GCCAATCGCAGGTAAGCAAC
Xbp1u	TCTGCAGCATCCAAAGCTGAC	GCATGTCTTGTAGAGTAGGC
Xbp1s	CTTGGATCTGCCGCAGGGTAT	GCATGTCTTGTAGAGTAGGC
BiP	ATATTACTGGCCGTCGTGGC	ACCAACGCAGGAATACGTGG
PDI	GACGGTGGACAACTTCAAGC	CTTGATGGGCGACTCCTTCTC
Edem1	GCGGATATGCAACGATTCGC	GACCCATCGTTGTGCAGGAA
Drs	AGTACTTGTTCGCCCTCTTCG	GGTCTCGTTGTCCCAGACG
BomS2	TGGCCAACGCTGTTCCC	CCTACTTTCCACCGTGCACAT
IM4	CAAGCCAACCAACAACCACC	ATGAGCACGGTTCCAGGTTG
IM14	TCTGCGGCTTTTTCTTCGCT	TTTGAATCAACGTGTGTCCGC
Generation of UAS-HA.mdy		
ENTR HA mdy-F	CACCATGTACCCATACGACGTCCCAGACTACGCTACCACCAATAAGGATCCCCAAGATAAG	
mdy-R	CTAACTACTGTAGTCGGTGCCGTTGA	

Table 1. Sequences of oligonucleotides used in this study.

Figure 1_Martinez et al.

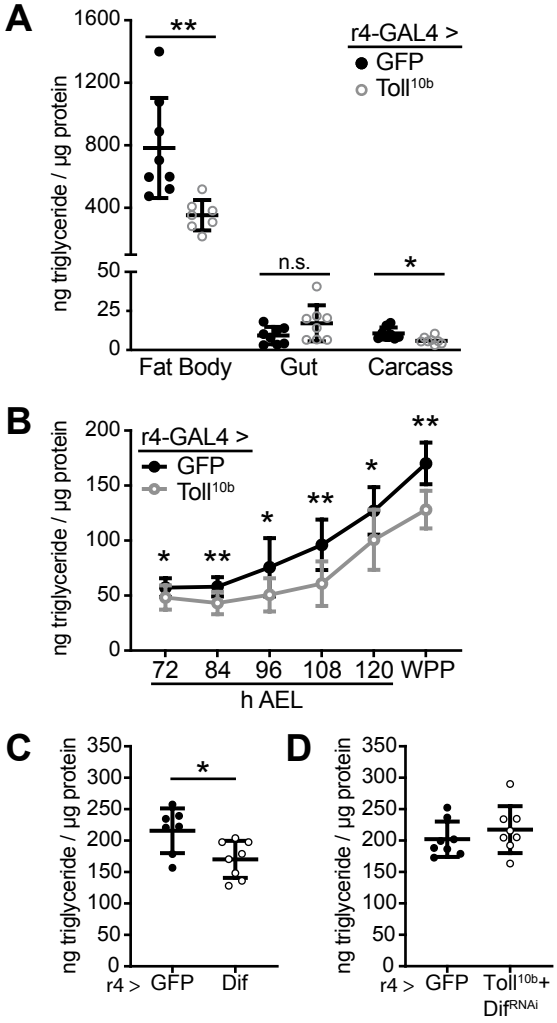

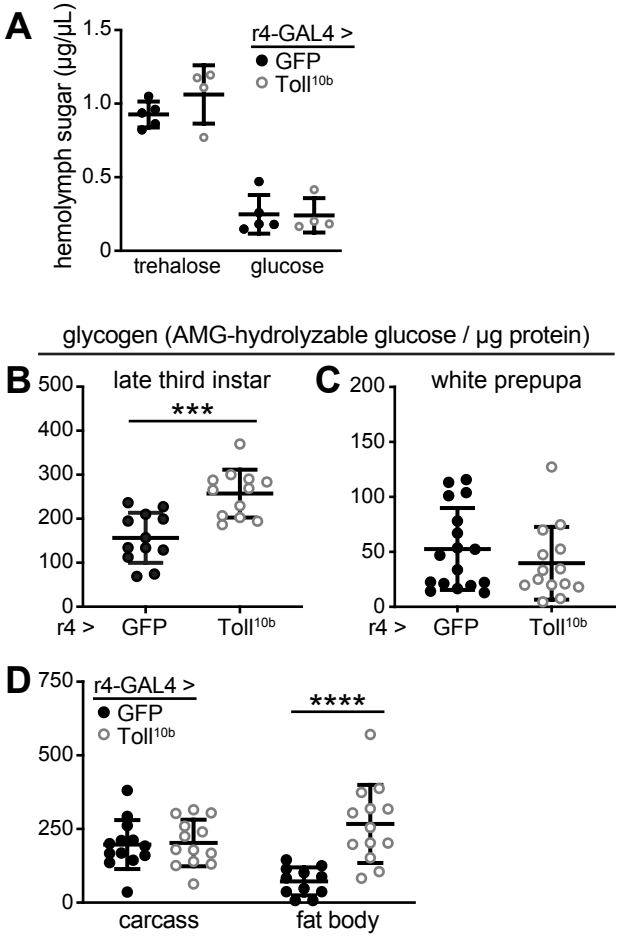

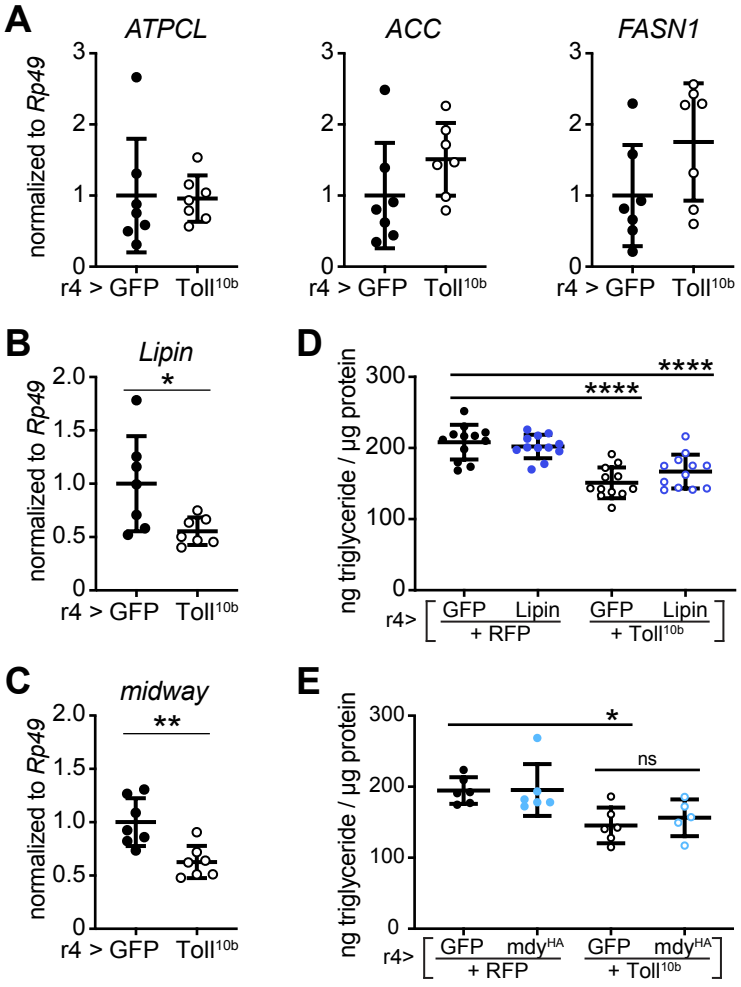

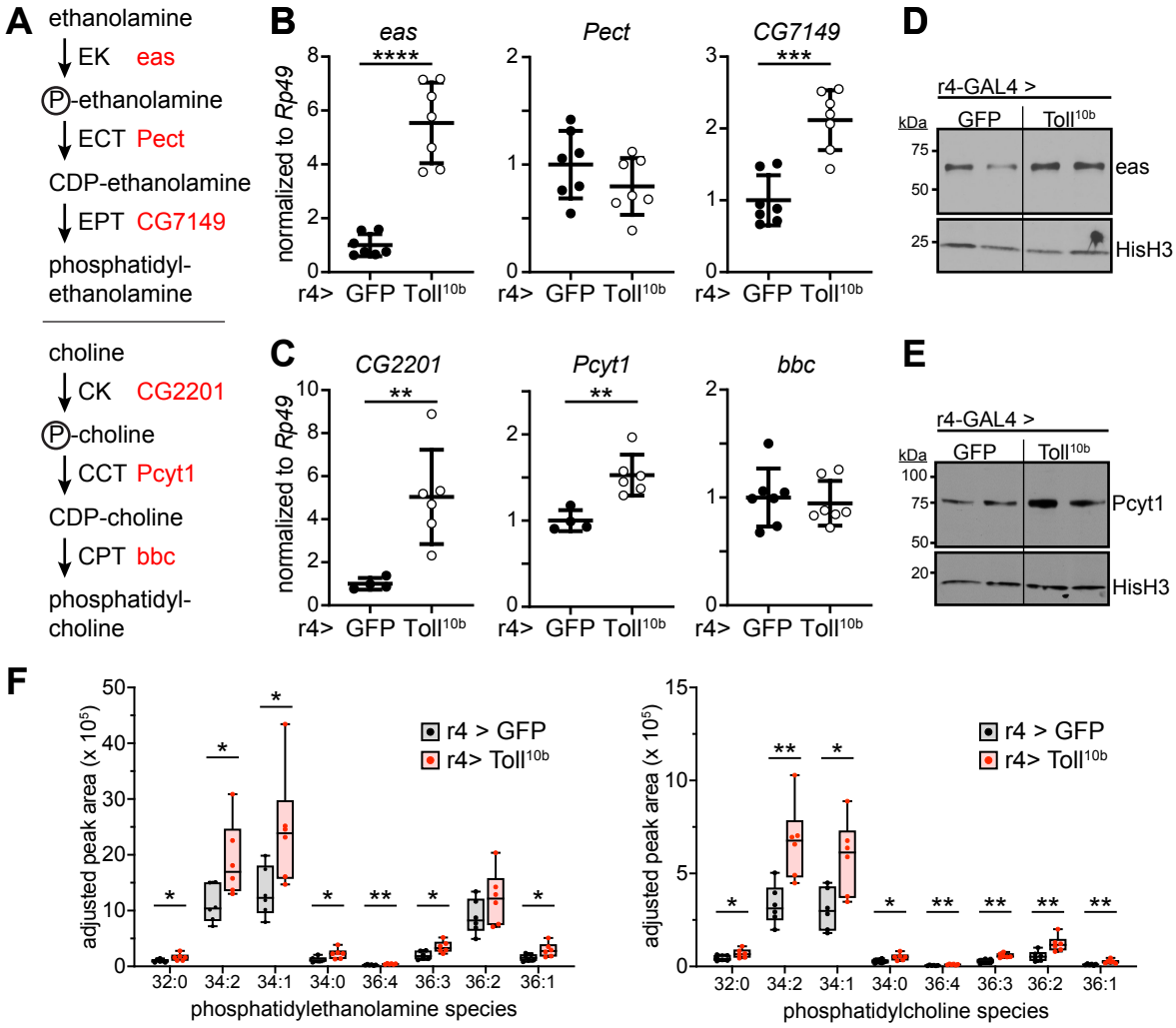

Figure 5_Martinez et al.

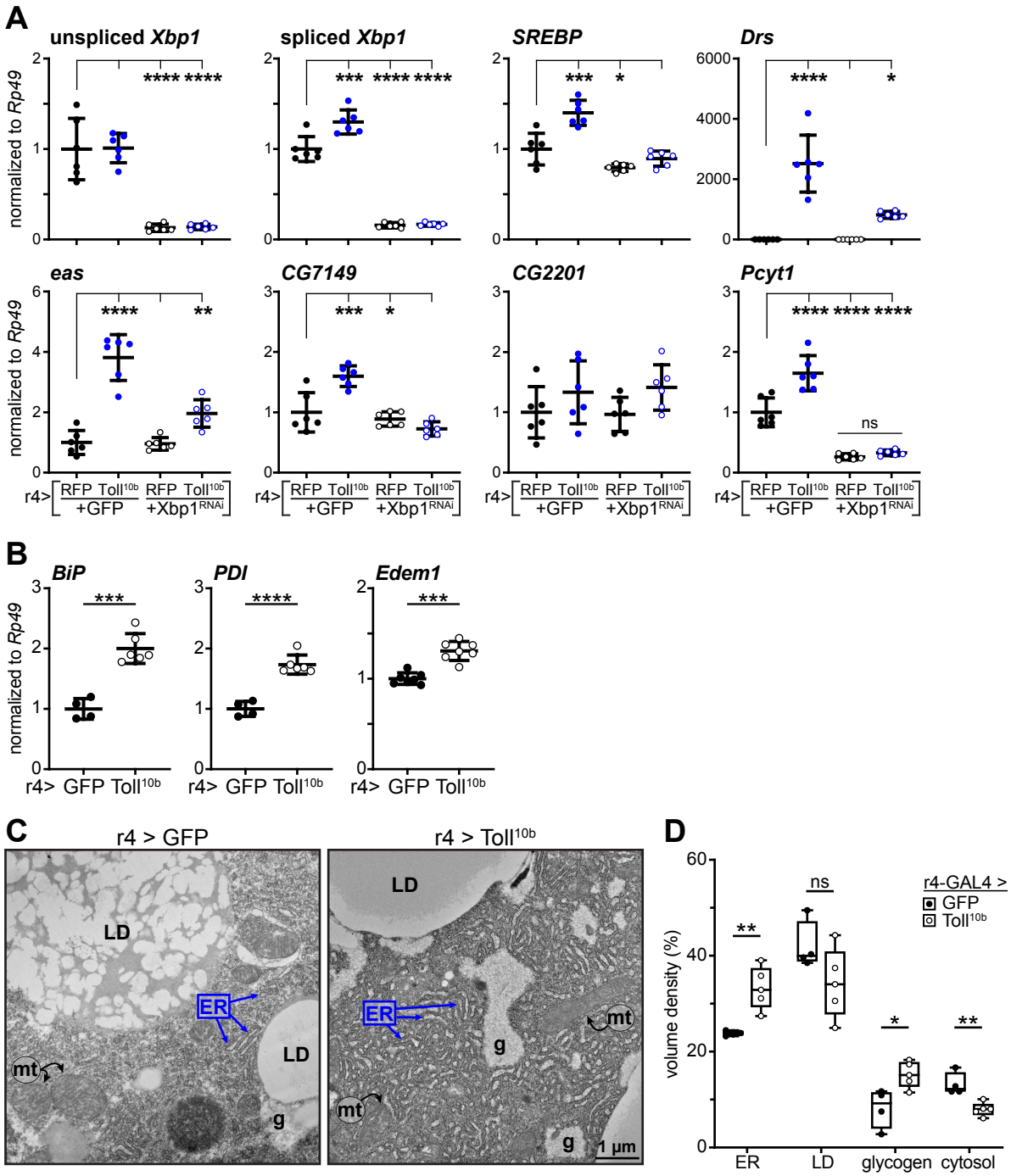

Figure 6_Martinez et al.